Robust Noninvasive Atrial Ectopic Beat Classification from Surface ECG using Second-order Statistics Blind Source Separation

Yingjing Feng[1,2], Caroline Roney[3], Mélèze Hocini[4], Steven Niederer[3], Edward Vigmond[1,2]

[1] IHU Liryc, Electrophysiology and Heart Modeling Institute, fondation Bordeaux Université, Pessac-Bordeaux, France
[2] Univ Bordeaux, IMB, UMR 5251, Talence, France
[3] Division of Imaging Sciences & Biomedical Engineering, King's College London, London, United Kingdom
[4] Bordeaux University Hospital (CHU), Electrophysiology and Ablation Unit, Pessac, France

Abstract

Ectopic Beats (EBs) generated from the atria or pulmonary veins, are an important trigger mechanism of atrial fibrillation (AF). They can be periodic, and have been commonly observed amongst AF patients in their initial episodes, as well as post-ablation. Robust non-invasive detection of EBs could improve the pre-operative prediction, as well as post-ablation management. By delaminating periodic components from body surface potential map using second-order statistics blind source separation (SOS-BSS) methods, EBs were extracted, and discriminated from stable AF rotors, another type of periodic source, the area-under curve of receiver operating characteristic (AUC-ROC) score of 0.92 was achieved over a synthetic dataset of 31 rotors and 58 EBs in LA, with and without Acetylcholine modulation.

1. Introduction

Atrial Ectopic Beats (EBs) arising from foci are an important mechanism of atrial fibrillation (AF), and have been commonly observed amongst AF patients in their initial episodes, as well as post-ablation. Robust non-invasive detection of EBs could improve the pre-operative planning for pulmonary vein isolation, and the assessment of EBs could be used for post-ablation monitoring.

Surface ECGs can be seen as sensor signals produced by a number of unknown sources. There exists a number of blind source separation (BSS) methods, based on assumptions that each source is statistically independent to each other, or there is some structure within the source. Second-Order Statistics (SOS) methods exploit covariance matrices with optimal linear predictability [1] to extract periodic sources from signals. Unlike most BSS algorithms which require additional steps to select the optimal number of components, they have less restriction in the selection of components, and the components can be ranked by their eigenvalues. Several works [2][3] adopted SOS methods to extract periodic atrial components, assuming AF signals over a short period exhibit quasi-periodicity, as well as to separate maternal from fetal ECG signals [4], but none was used to distinguish between different types of atrial periodic sources.

This study used a SOS-based algorithm to to analyze torso recordings to distinguish EBs from stable rotors, another major kind of periodic source underlying AF.

2. Methods

2.1. Modelling Rotors and EBs

We modelled spatiotemporally stable rotors and regular EBs, each lasting for 1000ms, in an anatomically realistic biatrial mesh with the CARPentry simulator [5], and computed surface potentials. The biatrial mesh was made from a scan of an AF patient of the CHU Bordeaux, with the addition of inter-atrial structures, as well as specification of regional eletrophysiological properties as in [6]. We ran monodomain simulations with lead positions shown in Fig. 1(e-f) to compute the standard 12-lead ECG, the 252-lead vest, and 2835-lead torso body surface potential maps (BSPMs) for each simulation. We first applied five stimuli at the sinoatrial node with an interval of 700ms to entrain the heart to sinus rhythm. We used $\alpha_{LA}, \beta_{LA}, \alpha_{RA}, \beta_{RA}$ of the universal atrial coordinate system [7] to specify location of conduction blocks (CBs) and stimulus sites on the left atrium (LA) and right atrium (RA).

Cross-field stimulation was used to initiate rotors (Fig. 2(a)): An S1 stimulus was first applied on an isthmus of $\alpha_{LA} = 0$, and after 225ms, when a third of LA tissue has been repolarised, an S2 stimulus was applied on nodes

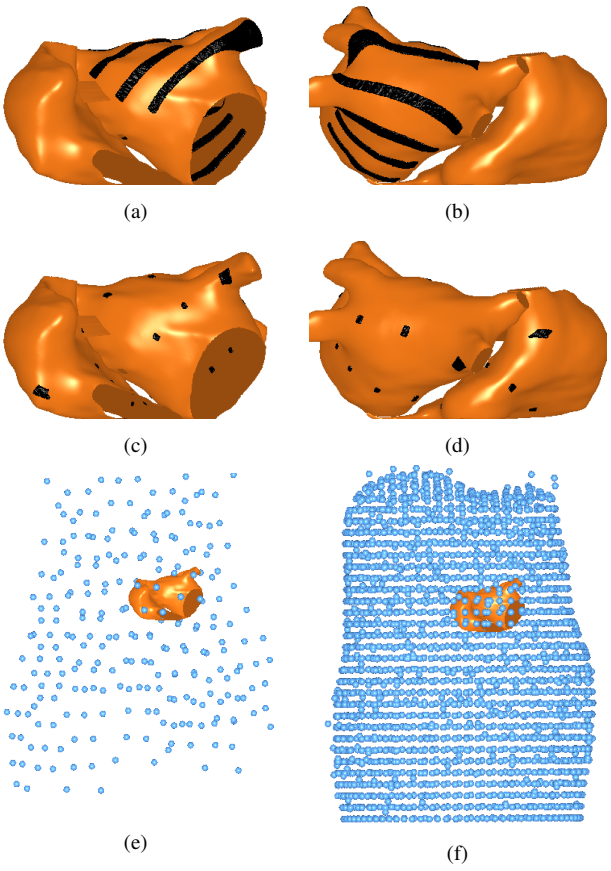

Figure 1: Locations for CBs (a-b), and foci (c-d). (e) Vest leads. (f) Torso leads.

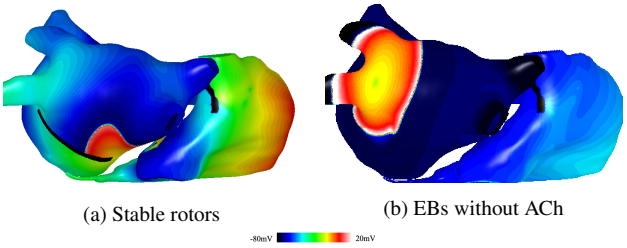

Figure 2: The transmembrane voltage of posterior LA for simulated atrial rotor and EBs. (a) An AF rotor is anchored around a CB (black line), where the CB is defined as a line joining the $\beta_{LA} = 0.2$, and $\alpha_{LA} \in [0.2, 0.8]$. (b) AF focus originating from ($\alpha_{LA} = 0.6, \beta_{LA} = 0.4$).

of β_{LA} ranging 0 up to $CB(\beta_{LA}) \in \{0.1, 0.2, \ldots, 0.8\}$. Anatomical CBs were also added on the LA, where β_{LA} of each CB corresponded to $CB(\beta_{LA})$, and α_{LA} from $0.2-0.8$, $0.3-0.7$, $0.4-0.6$ and $0.3-0.5$. Only those that maintained stable rotors ($\geq$2000ms) were analysed, 31 in total.

EBs (Fig. 2(b)) were triggered every 100ms at foci of approximately 2mm radius in the LA and RA, centered at combinations of (α,β) where $\alpha, \beta \in \{0.2, 0.4, 0.6, 0.8\}$, for a total of 29 simulations. We also performed simulations with electrophysiological hetrogeneity by including islands of Acetylcholine (ACh) release in the LA, including the appendage as in [8], wherein [ACh]$= 1\mu m$.

2.2. Classification of EBs with SOS-BSS

To apply SOS-BSS methods, we assume the signals $X = \{x_1, x_2, x_3, ...\}$ come from a number of unknown sources $S = \{s_1, s_2, s_3, ...\}$, so that $X = WS$. We first define the cumulant matrix with a time lag τ, $C_x(\tau) = E[x(t+\tau)x(t)^T]$. To recover $S \approx U^T W$, is to maximize the periodicity of a source $S_i, i = 1, 2, \ldots,$ which is to minimize the following measure:

$$\epsilon(\mathbf{w}, \tau) = \frac{\sum_{\mathbf{t}} |\mathbf{s(t+\tau)} - \mathbf{s(t)}|^{\mathbf{2}}}{\sum_{\mathbf{t}} |\mathbf{s(t)^2}|} = \mathbf{2}\left[\mathbf{1} - \frac{\mathbf{w^T C_x(\tau) w}}{\mathbf{w^T C_x(0) w}}\right].$$

The matrix column u_i from $U = \{u_1, u_2, \ldots\}$ is an eigenvector which diagonalizes the cumulant matrix. To solve for u_i, we first introduced AMUSE [9]. according to Rayleigh–Ritz theorem, it follows that the vector $\mathbf{w}$ minimizing $\epsilon(\mathbf{w}, \tau)$ is given by the eigenvector corresponding to the largest eigenvalue of the matrix pair $(C_x(\tau), C_x(0))$ of generalized eigenvalue decomposition. However, AMUSE heavily relies on an accurate estimation of the time lag τ for $C_x(\tau)$.

To estimate $C_x(\tau)$ reliably, we used SOBI [10] algorithm, a generalized version of AMUSE to a large set of time lags $\tau = \tau_1, \tau_2, \ldots, \tau_K$, to extract periodic components of different spectra from the BSPMs. SOBI constructs K cumulant matrices $C_x(\tau_1), C_x(\tau_2), \ldots, C_x(\tau_K)$, and uses a Jacobi-like joint diagonalization (JD) method to estimate u_i for these cumulant matrices. For atrial periodic sources (foci and rotors), we used a wide range of time lags from 80ms to 320ms as in [2] to form the set of cumulant matrices. The component with time lag $\tilde{\tau}$ corresponding to the largest eigenvalue of JD was chosen as the estimated time lag of the principal periodic component, and was then fed back into AMUSE by setting $\tau = \tilde{\tau}$ to compute $C_x(\tau)$. The decomposed components by AMUSE were ranked, again, by their corresponding eigenvalues.

As the decomposed components from AMUSE are ranked by periodicity with time lag $\tilde{\tau}$, a robust way to assess the periodicity of each component with time lag $\tilde{\tau}$ was the auto-correlation function (ACF). The first few components have, naturally, high ACF values at time lag $\tilde{\tau}$, but for signals containing a simple periodic source such as EBs, the lower-ranked components will still preserve a relatively high ACF value at time lag $\tilde{\tau}$, whereas the lowest ranked components capture the noise. We computed the

accumulated ACF (AACF) of top-ranked K components, $AACF(K) = \Sigma_{i=1}^{K} ACF_i(\tilde{\tau})$ where K is the number of preserved AMUSE components, as a metric to assess the periodicity of signals at $\tilde{\tau}$ to classify ectopic sources.

3. Results

Typical simulations are shown in Fig.2. We decomposed the 12-lead ECG, 252-lead vest BSPM, and 2835-lead torso BSPM of each simulation into different numbers of periodic components, and calculated their ACF and their fast fourier transform (FFT) spectrogram. Fig. 3 show decomposed torso ECG signals of a rotor and an EB with homogeneous LA surface, in which the lower-ranked components were more organised in EBs compared to stable rotors.

The corresponding AUC-ROC values using AACF of the top K out of total N components ($5 \leq N \leq 9$ to account for ECG with a smaller rank (≤ 9) of cumulant matrices) are shown in Fig. 4. We also added Gaussian noises with standard deviation $\sigma \in \{0, 0.1, 0.5\}$ on each lead, representing zero, middle and high-level noise. The AUC-ROC scores over all conditions are 0.87 ± 0.05, respectively, and averaging the AUC-ROC and their cut-off thresholds across all recording systems and noise levels, the maximal AUC-ROC score is 0.90 comes from with EBs threshold as $AACF(3) \geq 2.79$.

We compared our result with the power density degree of the dominant frequency (DF) $AFFTr_{2DF}$ [11], using the ratio of integral of 0Hz to $2 \times DF$ to the integral of 0Hz to 50Hz in the FFT spectrograms for classification, received AUR-ROC of 0.47, 0.52, and 0.50, respectively.

The complexity for the algorithm mainly comes from JD. On a Intel® Xeon® Gold 6140 Processor, the computation time for JD varied between 0.01 to 10 seconds for a 1000-sample ECG signal.

4. Discussions

Our algorithm achieved a maximal AUC-ROC score of 0.92 for all noise-free and medium- and high-noise conditions, outperforming the FFT-based $AFFTr_{2DF}$ metric. This is because DF is hard to pick, especially for complex FFT spectrograms, and single-lead FFT-based methods are easily corrupted by noise. By comparison, our method distinguished periodic signals from multiple leads simultaneously, robust to Gaussian noise for what we measured as up to 0.5. All AUC-ROC scores in Fig. 4 converge for $K \geq 5$, and variance increased with the level of Gaussian noise, showing the insensitivity to the number of components.

Pairwise paired t-tests ($p < 0.01$) suggest that both ECG and vest outperformed the torso for low and medium K under medium- and high-noise settings and little difference with a high K: ECG $>$ torso for $\sigma = 0.1, K = 1$ and for $\sigma = 0.5, K = 1, 2, 8$; vest $>$ torso for $\sigma = 0.1, K = 4, 5$ and for $\sigma = 0.5, K = 2$; ECG $>$ vest for $\sigma = 0.1, 0.5, K = 1$, suggesting that the standard ECG was sufficient, and a high K is preferable.

Future development will apply the method to patient signals and assess the correlation of EB occurence with ablation outcomes, and associate the spatio-temporal pattern of the recovered signals with the locations of EBs and rotors.

5. Conclusions

On simulations of stable rotors and regular EBs, regardless of the heterogeneity of LA surface, our SOS-based method shows advantages in combining multi-lead signals to identify different types of periodic source in AF over the single-lead FFT analysis method. The method is easy to use, robust to Gaussian noise, and insensitive to the number of components as well as ECG recording systems, making it suitable for low-cost pre-ablation assessment and post-ablation management.

Acknowledgments

Funding has been received from the European Union Horizon 2020 research and Innovation programme "Personalised In-silico Cardiology (PIC)" under the Marie Sklodowska-Curie grant agreement No 764738, and the French National Research Agency (ANR-10-IAHU-04).

References

[1] Puntonet CG, Lang EW. Blind source separation and independent component analysis, 2006.

[2] Castells F, Rieta J, Millet J, Zarzoso V. Spatiotemporal Blind Source Separation Approach to Atrial Activity Estimation in Atrial Tachyarrhythmias. IEEE Transactions on Biomedical Engineering feb;(2):258–267. ISSN 0018-9294.

[3] Llinares R, Igual J. Exploiting periodicity to extract the atrial activity in atrial arrhythmias. Eurasip Journal on Advances in Signal Processing ;(1). ISSN 16876180.

[4] Sameni R, Jutten C, Shamsollahi M. Multichannel Electrocardiogram Decomposition Using Periodic Component Analysis. IEEE Transactions on Biomedical Engineering aug;(8):1935–1940. ISSN 0018-9294.

[5] Vigmond EJ, Hughes M, Plank G, Leon L. Computational tools for modeling electrical activity in cardiac tissue. J Electrocardiol Dec. 2003;36(SUPPL.):69–74.

[6] Labarthe S, Bayer J, Coudière Y, Henry J, Cochet H, Jaïs P, Vigmond E. A bilayermodel of human atria:mathematical background, construction, and assessment. Europace 2014; 16(May):iv21–iv29. ISSN 15322092.

[7] Roney CH, Pashaei A, Meo M, Dubois R, Boyle PM, Trayanova NA, Cochet H, Niederer SA, Vigmond EJ. Universal atrial coordinates applied to visualisation, registra-

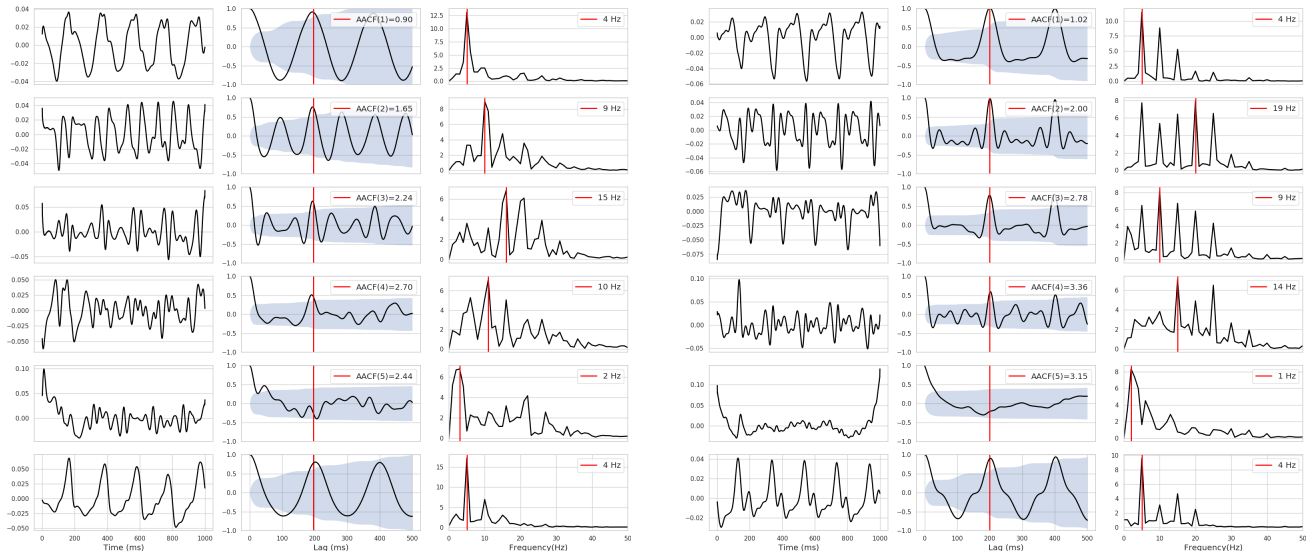

(a) stable AF rotor

(b) EB on homogeneous LA

Figure 3: Decomposition of noise-free torso signals into five components using our methods. The first five rows show the top five components as ranked by their eigenvalues, with the bottom row showing the V1 ECG, for stable AF rotors and EBs on homogeneous LA. The first column shows the decomposed signal, the second shows ACF(τ) lags where the red vertical bar marks $\tilde{\tau}$ with 95% confidence interval being shaded, and the third is the FFT spectrogram with DF in red.

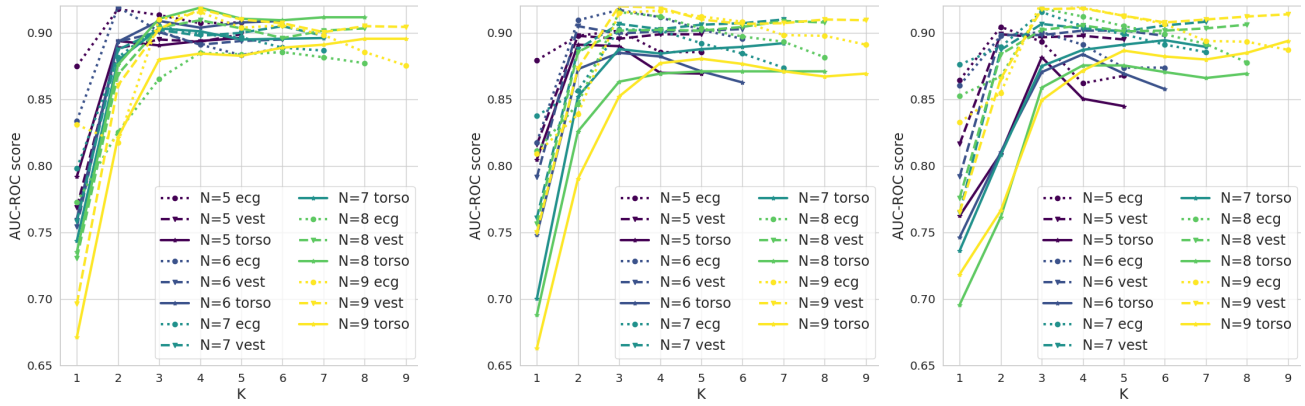

(a) Noise-free

(b) Gaussian white noise with $\sigma = 0.1$

(c) Gaussian white noise with $\sigma = 0.5$

Figure 4: AUC-ROC scores of AACF(K) out of N components for decomposition, regarding to three noise levels.

tion and construction of patient specific meshes. Medical Image Analysis jul 2019;55:65–75. ISSN 13618423.

[8] Bayer JD, Boukens BJ, Krul SP, Roney CH, Driessen AH, Berger WR, van den Berg NW, Verkerk AO, Vigmond EJ, Coronel R, de Groot JR. Acetylcholine Delays Atrial Activation to Facilitate Atrial Fibrillation. Frontiers in Physiology sep;1105. ISSN 1664042X.

[9] Tong L, Soon VC, Huang YF, Liu R. AMUSE: A new blind identification algorithm. Proceedings IEEE International Symposium on Circuits and Systems 1990;3:1784–1787. ISSN 02714310.

[10] Belouchrani A, Abed-Meraim K, Cardoso JF, Moulines E. A Blind Source Separation Technique Using Second-Order Statistics. Technical Report 2, 1997.

[11] Alday EAP, Colman MA, Langley P, Zhang H. Novel non-invasive algorithm to identify the origins of re-entry and ectopic foci in the atria from 64-lead ECGs: A computational study. PLOS Computational Biology mar;(3):e1005270. ISSN 1553-7358.

Address for correspondence:

Yingjing Feng
IHU Liryc, F-33600 Pessac-Bordeaux, France
yingjing.feng@ihu-liryc.fr